Stability and Flexibility in the Structure of the Hyperthermophile DNA-Binding Protein Sac7d†

Mebrahtu A. Kahsai, Ewan Martin, Stephen P. Edmondson, and John W. Shriver*

Laboratory for Structural Biology, Departments of Chemistry and Biological Sciences, Graduate Program in Biotechnology and Bioengineering, University of Alabama in Huntsville, Huntsville, Alabama 35899

Received June 16, 2005; Revised Manuscript Received August 4, 2005

ABSTRACT: Sac7d is a chromatin protein from the hyperthermophile *Sulfolobus acidocaldarius* that severely kinks duplex DNA with negligible change in protein structure. In previous work, the overall stability of Sac7d has been well-characterized with a global analysis of the linkage of folding, protonation, and anion binding. We extend that work here with NMR measurements of global stability as well as the distribution of stability and flexibility in the solution structure. Native state amide hydrogen exchange has been used to identify the most-protected core amide protons which exchange through global unfolding. The pH and temperature dependence of stability defined by native state exchange is in excellent agreement with the free energy surface determined by a linkage analysis of the dependence of folding on pH, salt, and temperature. These results confirm that the ΔC_P obtained from a Kirchhoff analysis of DSC data (i.e., ΔH vs T_m) is incorrect, and an accurate description of the protein stability curve for Sac7d requires a measure of the thermodynamic contributions of protonation and anion binding. Amide hydrogen exchange, along with generalized order parameters determined by ^{15}N relaxation data, demonstrates considerable variation in stability throughout the structure with some of the least stable regions occurring at the N- and C-termini. The most stable and inflexible region of the backbone occurs primarily in the DNA-binding β-sheet which is responsible for bending DNA.

Sac7d from the hyperthermophile *Sulfolobus acidocaldarius* binds nonspecifically to the minor groove of duplex DNA (*1*−*3*). The 7600 Da (66 residue) protein is generally believed to function as a chromatin protein in *Sulfolobus*, a crenarchaeota which lacks the true histones that have been described in other Archaea (*4*, *5*). Sac7d binds DNA as a monomer with a site size of about 4 base pairs and induces one of the largest kinks observed for any DNA-binding protein with a roll angle of approximately 66° at a single base pair step (*6*). Although the protein can significantly distort duplex DNA, there is negligible change in the protein structure (*7*). These observations coupled with the high thermal stability of the protein make Sac7d an excellent model system for studying the fundamental energetics of protein−DNA binding and distortion (*8*, *9*). To understand the interplay of forces responsible for DNA distortion, it is necessary to accurately define the global stability of the protein as well as the distribution of stability and flexibility in the DNA-binding site.

Thermal unfolding followed by CD and also scanning calorimetry have been used to map the global stability of Sac7d as a function of temperature (0−100 °C), pH (0−8), and salt concentration (0−0.3 M) (*10*, *11*). Sac7d is unusual in that protonation and anion binding promote the native fold at low pH, and two-state unfolding can be observed to pH 0. A global analysis of the stability data using a model which includes the linkage of folding, protonation, and anion binding indicates an intrinsic ΔC_P of unfolding which is significantly different from that obtained from a more traditional Kirchhoff analysis (*12*). One of the goals of this work was to use native state amide hydrogen exchange to obtain an independent measure of the stability of Sac7d as a function of pH and temperature to determine the accuracy of the linkage analysis.

Protein stability is often described in terms of the thermodynamics of global unfolding (*13*−*19*). Reversible two-state (N ↔ U) unfolding has been typically monitored using thermal denaturation, scanning calorimetry, and chemical denaturation (*20*−*26*). However, global stability measurements of unfolding can be deceptive in that unknown reactions coupled to unfolding may not be included in the analysis (*27*). In addition, global stabilities do not reflect fluctuations and local unfolding (*28*). Two-state global unfolding does not preclude local instability and unfolding due to fluctuations in the ensemble of folded states (*20*, *29*−*31*). Native state hydrogen exchange experiments have demonstrated that the stability of a protein is not described by a single set of parameters throughout the structure (*32*−*35*). Rather, a set of core residues unfold with a free energy representing global unfolding, while the remaining residues surrounding the core are involved in less stable structures which open or unfold more readily (at lower energy). Hydrogen exchange data therefore provide both a measure of global stability (represented by the core) as well as a delineation of the less stable regions of the structure.

† This work was supported by Grant GM49686 from the National Institutes of Health to J.W.S. and S.P.E.

* Address correspondence to John W. Shriver, Department of Chemistry, Materials Science Building, John Wright Drive, University of Alabama in Huntsville, Huntsville, AL 35899. Phone: 256-824-2477. Fax: 256-824-6349. E-mail: shriverj@uah.edu.

10.1021/bi051167d CCC: $30.25
Published on Web 09/22/2005

Amide hydrogen exchange in proteins results from the exposure of an amide NH to solvent due to either local or global unfolding (*35*, *36*). Hydrogen exchange data is typically analyzed using the following model in which unfolding disrupts a hydrogen bond making the exposed NH available for exchange:

$$\mathrm{NH(closed)} \underset{k_{cl}}{\overset{k_{op}}{\rightleftharpoons}} \mathrm{NH(open)} \xrightarrow{k_{ch}} \mathrm{exchanged}$$

where k_{op} and k_{cl} are the opening and closing rate constants for the local unfolding reaction, and k_{ch} is the intrinsic exchange rate for the exposed NH (*37*). The observed exchange rate constant is given by

$$k_{obs} = \frac{k_{op}k_{ch}}{k_{cl} + k_{ch}} \quad (1)$$

If the intrinsic exchange rate is slower than the closing rate ($k_{cl} \gg k_{ch}$), then the so-called EX2 exchange kinetics prevails, and

$$k_{obs} = \frac{k_{op}}{k_{cl}}k_{ch} = K_{op}k_{ch} \quad (2)$$

Under these conditions, the pH dependence of k_{obs} is dictated primarily by the pH dependence of k_{ch}, and a plot of log k_{obs} versus pH is a chevron with a slope of 1 above a minimum around pH 4 (base-catalyzed exchange) and a slope of -1 at lower pH (acid-catalyzed exchange) (*29*, *38*). The ratio of k_{ch}/k_{obs} is referred to as the protection factor (PF)[1] and is equal to the inverse of the equilibrium constant, K_{op}, for opening the structure protecting the NH. In this model, the free energy change associated with the equilibrium constant is therefore given by

$$\Delta G^{o}_{HX} = -RT \ln\left(\frac{k_{obs}}{k_{ch}}\right) \quad (3)$$

where the symbol ΔG^{o}_{HX} is used to distinguish the free energy change from that obtained from more direct thermodynamic measurements (e.g., calorimetry). A set of "core" amide protons in the protein require global unfolding to expose the NHs so that the measured ΔG^{o}_{HX} for these protons can provide a measure of the global stability. This is only true for NHs undergoing EX2 exchange kinetics. If $k_{cl} \ll k_{ch}$ (high pH or low stability), then EX1 kinetics exists. Under these condition $k_{obs} = k_{op}$, and eq 3 is invalid. Amide protons in the EX1 regime have exchange rates which are essentially pH-independent. The EX2 kinetics is most easily demonstrated by the pH dependence of the exchange rate (*35*, *38*, *39*).

In the results presented here, we use native state hydrogen exchange to define the temperature and pH dependence of Sac7d stability. Native state hydrogen exchange stability data for the core residues are consistent with that obtained using a linkage analysis. Amide exchange data also provide a mapping of the distribution of stability in the structure which coincides with the backbone mobility indicated by ^{15}N heteronuclear relaxation data.

[1] Abbreviations: DSC, differential scanning calorimetry; HX, hydrdogen exchange; NOE, nuclear Overhauser effect; PF, protection factor; R_1, longitudinal relaxation rate ($1/T_1$); R_2, transverse relaxation rate ($1/T_2$); τ_m, overall rotational correlation time; T_1, longitudinal relaxation time; $T_{1\rho}$, rotating frame relaxation time; T_2, transverse relaxation time.

MATERIALS AND METHODS

Protein Purification and NMR Sample Preparation. The sac7d gene in a pET-3b expression vector was expressed in *Escherichia coli* BL21(DE3)pLysS cells (*1*) in minimal media supplemented with $^{15}NH_4Cl$ (Isotec). ^{15}N-Enriched recombinant protein was purified as described (*1*), extensively dialyzed against deionized water, and lyophilized.

Amide Hydrogen Exchange Experiments. ^{1}H,^{15}N HSQC spectra were collected on a Varian 500 MHz (11.7 T) NMR spectrometer with a 5 mm triple resonance probe equipped with *z*-axis shielded gradients. Spectra were collected with minimal perturbation of the water spin populations using sensitivity-enhanced pulsed field gradient selection (*40*). Spectral widths were typically 6000 Hz in the ^{1}H dimension and 1700 Hz in the ^{15}N dimension, with 512 and 256 complex points in the ^{1}H and ^{15}N dimensions, respectively. Four transients were collected for each t_1 increment to give a total data acquisition time per spectrum of 40 min.

NMR samples for hydrogen exchange experiments were prepared by dissolving approximately 5 mg of lyophilized protein in 700 μL of 99.9% D_2O (Sigma) containing 0.3 M KCl and 10 mM potassium acetate. The pH was adjusted to the desired value with DCl (Sigma) or NaOH in D_2O. Unless indicated otherwise, reported pH values in D_2O were not adjusted for the deuterium isotope effect. The time of protein−buffer mixing was recorded as the initiation time of the exchange process. In studies of the temperature dependence of exchange, separate NMR samples were stored and data were collected at identical specified temperatures. In native state hydrogen exchange experiments, the GdnHCl concentration in NMR samples was adjusted gravimetrically using a 3.7 M stock solution of GdnHCl, and the concentration of the stock GdnHCl solution was measured by refractometry (*23*).

Hydrogen Exchange Data Analysis. NMR data were processed using FELIX (Accelrys, San Diego, CA). ^{1}H,^{15}N HSQC 2D spectra were zero-filled to 1024 × 512 data points. Apodization of both the ^{1}H and ^{15}N dimensions was performed using a shifted sine bell squared function. ^{1}H,^{15}N HSQC peak assignments for Sac7d have been published previously (*41*). Peak intensities were quantified by volume integration, and the time dependence of the volumes were fit to a first-order exponential function $V(t) = V_o + V_i \exp(-k_{obs}t)$ to obtain the exchange rate constants, k_{obs}. The intrinsic rate constant, k_{ch}, for each amide proton at a specific pH and temperature was calculated using the equations from Bai et al. (*42*). The apparent free energies of unfolding determined by hydrogen exchange rates were calculated using eq 3.

The temperature dependence of the free energy of unfolding (i.e., the protein stability curve (*16*)) was defined by an integrated form of the Gibbs−Helmholtz equation (*15*, *19*):

$$\Delta G^{\circ}(T) = \Delta H^{\circ}\left(\frac{T_m - T}{T_m}\right) - (T_m - T)\Delta C_p + T\Delta C_p \ln\left(\frac{T_m}{T}\right) \quad (4)$$

with three parameters: the enthalpy of unfolding (ΔH) at the midpoint temperature (T_m) and the change in heat capacity associated with unfolding (ΔC_P). Temperatures of maximal stability, T_{max}, were obtained by locating the maximum of ΔG, ΔG_{max}, using *Mathematica* (Wolfram Research). Errors in the parameters were propagated using standard propagation formulas (*43*).

^{15}N Relaxation and NOE Measurements. ^{15}N T_1, ^{15}N $T_{1\rho}$, and {^{1}H}-^{15}N NOE measurements were performed on Sac7d (20 mg/mL, pH 4.6, 90% H_2O/10% D_2O) at 11.7 T using pulse sequences kindly provided by Dr. Lewis Kay (University of Toronto) (*44*, *45*). ^{15}N T_1 relaxation data were collected with delay times of 0.04, 0.08, 0.12, 0.16, 0.21, 0.27, 0.33, 0.40, 0.48, and 1.2 s, with a delay of 3 s between sequence cycles. ^{15}N $T_{1\rho}$ relaxation data were collected with delays of 0.01, 0.02, 0.03, 0.04, 0.05, 0.06, 0.08, 0.1, and 0.12 s, with a 3 s delay between sequence cycles. Suppression of cross-correlation effects in ^{15}N $T_{1\rho}$ experiments was obtained using a train of phase alternated ($x,-x$), random length ^{1}H pulses applied during the ^{15}N spin lock as described (*45*). ^{1}H saturation for {^{1}H}-^{15}N NOE measurements was obtained using a train of 120° ^{1}H pulses with 5 ms separation and a saturation time of 5 s. A total delay of 10 s was used between sequence cycles for both saturated (5 s delay + 5 s saturation) and unsaturated (10 s delay) experiments. Duplicate {^{1}H}-^{15}N NOE, T_1, and $T_{1\rho}$ experiments at three different delay times were used to estimate uncertainties in peak intensities in the three types of experimental data. Peak intensities and errors were extracted using FELIX macros.

{^{1}H}-^{15}N NOE and ^{15}N Relaxation Data Analysis. T_1 and $T_{1\rho}$ peak intensities were fit with the CURVEFIT module of ModelFree kindly distributed by A. G. Palmer (Columbia University) (*46*). R_2 relaxation rates were calculated from $R_{1\rho}$ rates as described (*45*). A global rotational correlation time (τ_m) was obtained using the method proposed by Kay et al. (*47*) as implemented in routines distributed by A. G. Palmer. An overall rotational correlation time was also obtained by optimization of the global diffusion model using only those ^{1}H,^{15}N pairs in defined secondary structure. The extent to which rotational motion was anisotropic was investigated using the quadric_diffusion program distributed by A. G. Palmer. Order parameters describing backbone flexibility were obtained from {^{1}H}-^{15}N NOE and ^{15}N T_1 and T_2 relaxation data using ModelFree v.4.15 with an isotropic rotational diffusion model.

RESULTS

Amide Hydrogen Exchange and Definition of Core Residues. Native state amide hydrogen/deuterium exchange in Sac7d was followed using ^{1}H,^{15}N-HSQC NMR spectra for up to 7 months after dissolution of the protein in D_2O buffer. A considerable variation in exchange rates was observed (Figure 1), with 30 of the possible 64 amide hydrogens exchanging at least 2 orders of magnitude more slowly than observed in model peptides. The EX2 exchange kinetics was demonstrated for the slowest NHs by monitoring the pH dependence of the exchange rate at 30 °C, the highest temperature used in this work. A plot of log(k_{obs}) values for the most slowly exchanging amide hydrogens at pH 6.4 versus log(k_{obs}) values at pH 5 was linear with a slope of 1.0 ($R = 0.99$) (data not shown). Similarly, a plot of log(k_{obs}) values at pH 1.99 versus those at pH 1.0 showed a slope of 0.89 ($R = 0.94$) (data not shown). Plots of log(k_{obs}) for slowest exchanging NHs versus pH showed a characteristic chevron-shaped dependence with a minimum near pH 4 (data not shown). The combined data showed a slope of approximately 1 above the minimum (viz. 0.86 ± 0.01), while that on the low-pH side was slightly less, with an average slope of -0.70 ± 0.07.

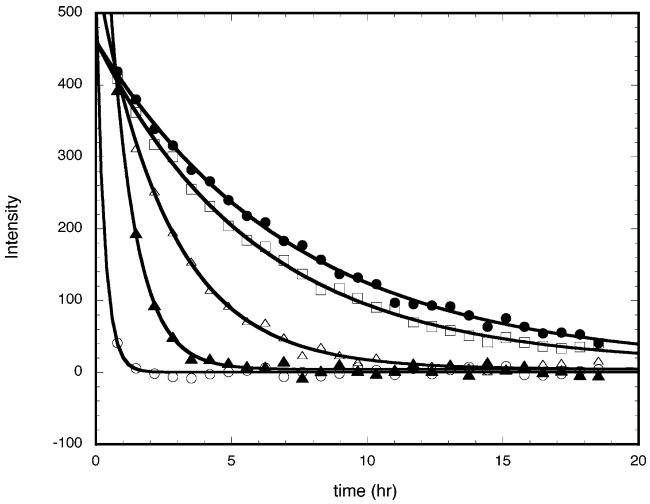

FIGURE 1: Representative hydrogen−deuterium exchange curves for selected amide protons in Sac7d (I20 (▲), V4 (○), W24 (●), V30 (□), and S31 (△)). Exchange data was obtained at 30 °C in 10 mM potassium acetate (pH 7.3) with 0.3 M KCl.

Table 1: Native State Amide Hydrogen Exchange Kinetics and Unfolding Free Energies for the Most Protected NHs in Sac7d at pH 5.0 and 30 °C

NH	k_{obs}[a] ($\times 10^{-5}$ min^{-1})	PF[b] (k_{ch}/k_{obs})	$\Delta G°_{HX}$[c] (kcal/mol)	$\Delta G°_{HX}$ (ext)[d] (kcal/mol)
W24	4.1 (0.5)	46 800 (5700)	6.47 (0.07)	6.54 (0.05)
V30	4.6 (0.6)	38 000 (4900)	6.35 (0.08)	6.44 (0.04)
S31	9.8 (0.5)	116 000 (5900)	7.02 (0.03)	7.00 (0.03)
F32	8.7 (0.5)	85 000 (4900)	6.83 (0.03)	6.75 (0.05)
T33	8.7 (0.5)	76 900 (4400)	6.77 (0.03)	6.72 (0.03)
Y34	18.0 (0.7)	32 000 (1200)	6.25 (0.02)	6.41 (0.06)
G43	24.7 (0.8)	85 000 (2800)	6.83 (0.02)	6.91 (0.05)
V45	2.4 (0.5)	56 300 (11 700)	6.59 (0.1)	6.57 (0.05)
L55	2.2 (0.1)	108 300 (4900)	6.98 (0.03)	6.87 (0.1)

[a] pH 5, 0.3 M KCl, 30 °C. Errors (standard deviations) obtained from nonlinear regression are shown in parentheses. [b] Protection factors (PF) are calculated using the predicted intrinsic exchange rates k_{ch} calculated according to Bai et al. (*42*). Errors in parentheses (standard deviations) are propagated from k_{obs}. [c] Hydrogen exchange free energies of local unfolding were obtained from eq 3 in the text. Errors (standard deviations) are propagated from k_{obs}. [d] Native state free energies of unfolding obtained by extrapolating the hydrogen exchange free energies as a function of GdnHCl to 0 M denaturant (Figure 2). Errors (standard deviations) are obtained from linear fits of the data.

The exchange kinetics of the nine most protected amide hydrogens (W24, V30, S31, F32, T33, Y34, G43, V45, and L55) with protection factors exceeding 10 000 is summarized in Table 1. Free energies for unfolding, $\Delta G°_{HX}$, were calculated from the hydrogen exchange rates using $\Delta G = -RT \ln(k_{obs}/k_{ch})$. The most protected NHs showed a linear dependence of $\Delta G°_{HX}$ on guanidine hydrochloride, and the native state free energies obtained by extrapolation to 0 M denaturant gave nearly identical values (6.7 ± 0.2 kcal/mol) (Figure 2). Less protected NHs (e.g., I20) showed a nonlinear dependence of $\Delta G°_{HX}$ on guanidine hydrochloride concen-

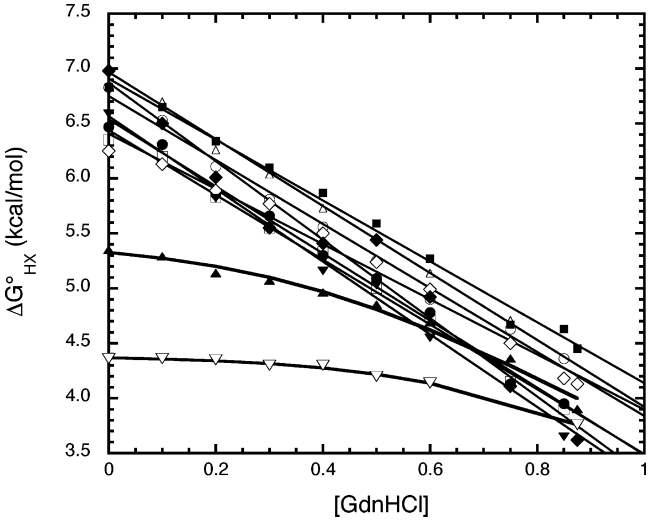

FIGURE 2: Dependence of the free energy of exchange on guanidine hydrochloride concentration for selected amide protons in Sac7d. The most slowly exchanging core protons show a linear dependence on GdnHCl (W24 (●), V30 (□), S31 (△), F32 (○), Y34 (◇), G43 (■), V45 (▼), and L55 (◆)), while the more rapidly exchanging amide protons (e.g., I20 (▲) and A44 (▽)) show a nonlinear dependence due to local fluctuations which merge with global unfolding at high GdnHCl. Data collected at pH 5.0, 30 °C, in 10 mM potassium acetate with 0.3 M KCl.

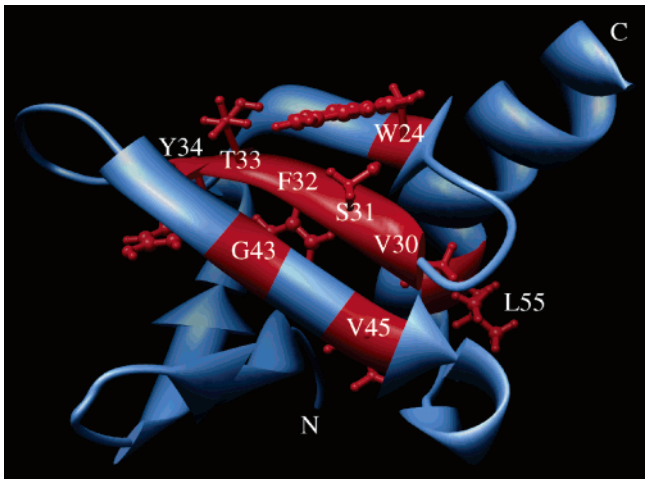

FIGURE 3: Structure of Sac7d showing the location of the nine residues with the most protected NHs indicated by native state hydrogen exchange. The N- and C-termini are labeled.

tration that deviated significantly from the more protected amide protons at lower concentrations of denaturant. Such a dependence is often attributed to contributions from local fluctuations (*28*). In contrast, the steeper, linear dependence of ΔG^{o}_{HX} on denaturant concentration observed for the most protected NHs indicates that exchange at these sites requires denaturant-induced global unfolding. This was supported by the observation that ΔG^{o}_{HX}values for this group at zero denaturant were comparable to, but slightly greater than, the unfolding free energy obtained for global unfolding published previously (*10*, *12*). The exchange data indicate that the most stable core of Sac7d is located largely in the DNA-binding, three-stranded β-sheet, along with additional contributions from the first turn of the C-terminal α-helix which packs against the β-sheet (Figure 3).

The ΔG°_{HX} values at zero denaturant for the most protected core NHs were somewhat greater than that determined

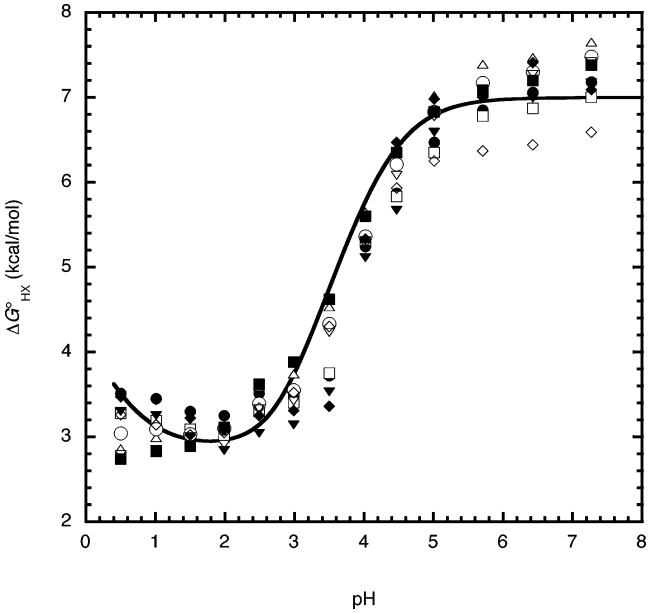

FIGURE 4: pH dependence of the hydrogen exchange free energies for amide protons of Sac7d core residues (W24 (●), V30 (□), S31 (△), F32 (○), T33 (▽), Y34 (◇), G43 (■), V45 (▼), and L55 (◆)). Data collected at 30 °C in 10 mM potassium acetate with 0.3 M KCl. The solid curve through the data is the predicted dependence of the unfolding free energy using the parameters from the global linkage analysis of stability data (*10*, *11*). The curve has been shifted vertically by +1.0 kcal/mol to adjust for the increase in stability due to D_2O (see text). The pH is that obtained from a glass electrode and has not been adjusted for the isotope effect.

previously for global unfolding using thermal denaturation experiments. This is explained by the enhanced stability conferred by D_2O in the hydrogen exchange experiments (*26*). DSC of Sac7d in D_2O at pH 7 (with 0.3 M KCl) showed a T_m of 92.8 °C and a ΔH of 65.5 kcal/mol, compared to 90.1 °C and 58.5 kcal/mol in H_2O. Using these values in the linkage model for Sac7d increased the calculated ΔG for unfolding at pH 5 and 30 °C (in 0.3 M KCl) from 5.8 to 7.0 kcal/mol, in good agreement with the measured ΔG^{o}_{HX}values (i.e., 6.7 ± 0.2 kcal/mol). The DSC and hydrogen exchange data indicate that D_2O increases the free energy of unfolding Sac7d by about 1 kcal/mol at 30 °C.

Mapping the Free Energy Surface for Sac7d Unfolding with Hydrogen Exchange. The ΔG^{o}_{HX} values for the nine most protected NHs (Y24, V30, S31, F32, T33, Y34, G43, V45, and L55) were monitored as a function of pH at 30 °C (Figure 4). The stabilities were essentially constant above pH 6, but a significant decrease was observed below pH 6. About half of the NHs showed a plateau in ΔG^{o}_{HX} below pH 2 (S31, F32, T33, and G43), while the others indicated a slight increase in stability below pH 2 (Y24, V30, Y34, V45, and L55). The observed pH dependence of stability was similar to the pH dependence of the T_m observed previously by DSC, especially the increase observed below pH 2 (*10*). The pH dependence of the stability was consistent with that obtained from a global linkage analysis of unfolding data obtained as a function of pH, salt, and temperature (Figure 4, solid line) (*10*).

The temperature dependence of ΔG^{o}_{HX} for Sac7d was determined from hydrogen exchange measurements from 5 to 30 °C at pH 7.95 and 0.3 M KCl (Figure 5). The data showed a broad stability curve with a maximum of ap-

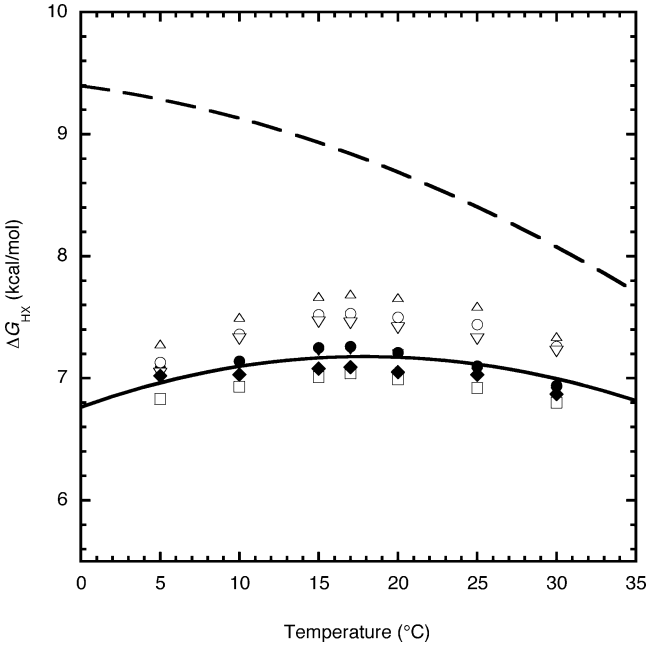

FIGURE 5: Temperature dependence of the hydrogen exchange free energies for amide protons of Sac7d core residues (W24 (●), V30 (□), S31 (△), F32 (○), T33 (▽), V45 (▼), and L55 (◆)). Data were collected in 10 mM potassium acetate (pH 7.95) with 0.3 M KCl. The calculated stability curve obtained from a global linkage analysis of the dependence of folding on temperature, pH, and salt is shown with the solid curve. For comparison, the stability curve obtained using thermodynamic parameters obtained from a Kirchhoff analysis of DSC data is shown with the dashed curve ($\Delta H = 58$ kcal/mol, $\Delta C_P = 500$ (cal/deg)/mol; $T_m = 91$ °C). Both curves have been shifted vertically by +1.0 kcal/mol to adjust for the effect of D_2O.

proximately 7.3 kcal/mol at 18.0 °C. The temperature dependence of ΔG^o_{HX} is in excellent agreement with that predicted by the global linkage analysis of thermal unfolding data if allowance is made for enhanced stability in D_2O, that is, a maximum in stability of 7.2 kcal/mol (6.2 + 1.0 kcal/mol) at 17.9 °C (solid curve, Figure 5). The hydrogen exchange data do not support the stability curve calculated using the ΔC_P obtained from a Kirchhoff analysis of DSC data (dashed curve). Nonlinear regression of the temperature dependence of the combined ΔG^o_{HX} values for the core NHs to an integrated form of the Gibbs−Helmholtz equation (see Materials and Methods) resulted in a ΔH of 74.1 (±8.5) kcal/mol, ΔC_P of 978 (±253) (cal/deg)/mol, with a T_m of 85.5 (±9.1) °C.

Backbone Flexibility and ^{15}N Relaxation. The backbone dynamics of Sac7d were characterized using ^{15}N NOE and relaxation data at 30 °C. Of the 64 possible amide NH vectors (66 residues minus the N-terminus and P51), 11 were eliminated from the final relaxation analysis: seven NH correlations (K2, F6, K39, N37, K22, D35, and K65) could not be sufficiently resolved for accurate measurement of relaxation times, and data for four (E62, D36, L54, and R63) could not be fit by any of the five models in ModelFree in initial trials. All of the relaxation data for the remaining 53 NH vectors could be fit as single exponential decays, and the R_1, R_2, and NOE data are summarized in Figure 6. The average R_1 and R_2 rates were 2.464 ± 0.247 and 5.172 ± 0.702, respectively, and the average R_2/R_1 ratio was 2.092 ± 0.195. The average NOE (excluding the small C-terminal

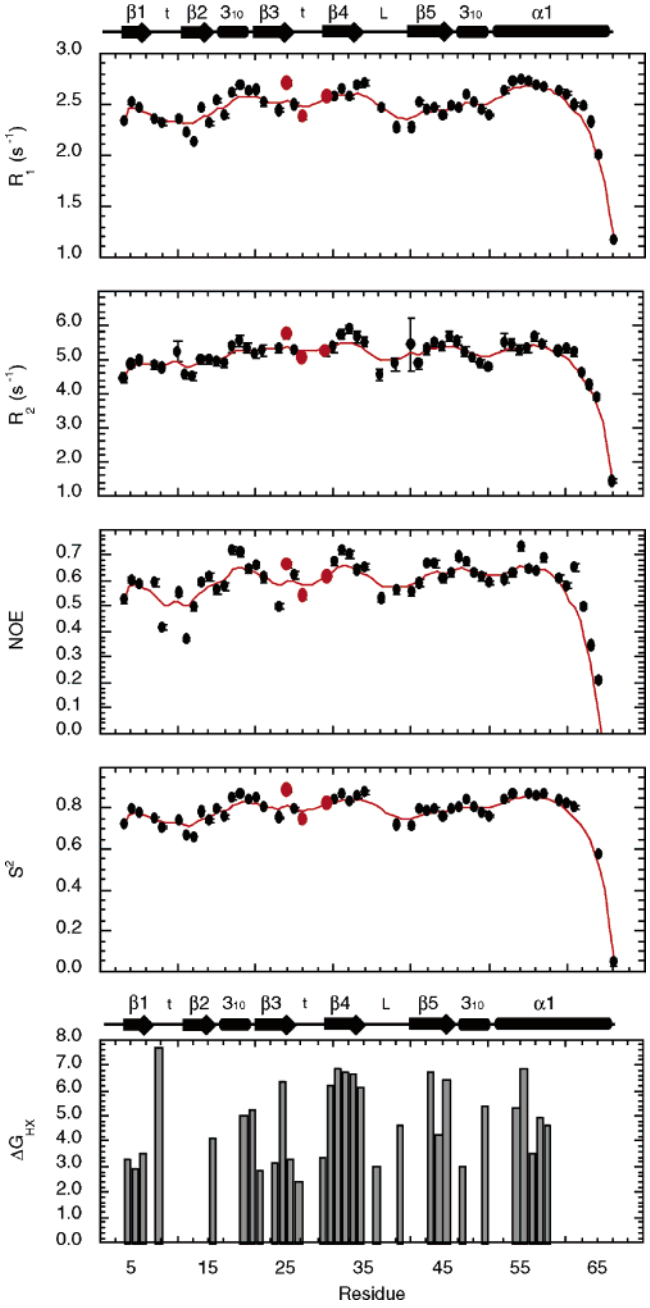

FIGURE 6: Sequence dependence of the ^{15}N heteronuclear relaxation rates, NOEs, and derived order parameters compared to the free energies of amide hydrogen exchange for Sac7d. A cartoon indicating the location of secondary structure in the sequence is indicated above the relaxation and stability data with five β-strands ($\beta1-\beta5$), one helix (α1), two 3_{10} helices (3_{10}), two tight turns (t), and a loop (L). Relaxation data for W24, M27, and V30 are highlighted in red. The line through the data is a spline fit to guide the eye and facilitate comparison to the secondary structure drawing.

NOEs for K64 and K66) was 0.607 ± 0.084, which is consistent with the size of Sac7d. The relaxation data for 32 NH vectors were selected using the criteria specified by Tjandra et al. (*48*) to obtain a global rotational correlation time τ_m of 3.70 ± 0.10 ns, in good agreement with that expected for isotropic rotation of Sac7d (i.e., at 25 °C τ_m(ns) ≅ MW(kDa)/2). The possibility of anisotropic rotation of the protein was investigated using the ^{15}N relaxation data with the program *quadric_diffusion* (A. G. Palmer, Columbia University). A $D_{||}/D_{\perp}$ ratio of 1.19 was obtained assuming

an axially symmetric model, but little benefit relative to an isotropic rotation model was indicated by the *F*-statistic. An analysis of ^{15}N relaxation data was therefore performed with an isotropic tumbling model. Errors resulting from assuming isotropic tumbling were minimized by characterizing the flexibility using generalized order parameters (*49*).

The ^{15}N relaxation data for each residue were fit using the "model free" formalism of Lipari and Szabo (*50*) as extended by Clore et al. (*51*) and implemented in ModelFree (*46*). An optimized fit of the data provided an overall rotational correlation time of 3.70 ± 0.02 ns. The generalized order parameters fell between a maximum of 0.891 (W24) and a minimum of 0.049 (K66). The average S^2 values over 52 of the 53 vectors used in the final analysis was 0.794 ± 0.069 (K66 was excluded in the average due to its low S^2). In general, the largest values for S^2 occurred for NHs in regions of secondary structure, in particular the 3_{10} helix between the β-ribbon and three-stranded β-sheet, the center strand of the β-sheet, and the beginning of the C-terminal helix. The most flexible regions occurred in the loops and turns between the regular secondary structural elements and also at the end of the C-terminal helix. Less mobility was observed at the N-terminus, with a significant S^2 observed starting with K3 (0.73). All of the ^{15}N relaxation data indicated that the C-terminal helix was increasingly flexible beyond R60, that is, the last 1.5 turns of helix which extend beyond the interface between the helix and β-sheet.

DISCUSSION

The enhanced stability of some thermophile proteins has been attributed to an optimization of packing and intermolecular interactions so that the functional state of the hyperthermophile protein is similar to that of a mesophile protein under optimal physiological conditions, that is, similar biophysical properties in "corresponding states" (*52*, *53*). This is generally believed to lead to increased rigidity of hyperthermophile proteins at temperatures that would be optimal for mesophile protein function. Similarly, the enhanced stability of some proteins has been attributed to increased stabilization of terminal sequences, thus, preventing an "unzipping" or fraying of the structure (*54*, *55*). Tests of these hypotheses have been limited by the small number of hyperthermophile proteins which are amenable to biophysical characterization of stability and flexibility, although the number of thermophile proteins which are known to unfold reversibly has increased considerably in the past few years (*56*−*62*). With the data presented here, there are now three hyperthermophile proteins for which thermodynamic measurements of reversible unfolding are complemented by molecular characterizations of flexibility: Sac7d from *Sulfolobus* (*10*−*12*), rubredoxin (RdPf) from *Pyrococcus furiosus* (*63*, *64*), and RNase H from *Thermus thermophilus* (*65*−*67*). The characterization of the stability of Sac7d is the most complete of the three, with data covering a broad range of temperature, pH, and salt concentrations. The thermal unfolding, hydrogen exchange, and backbone dynamics data present a consistent description of the stability and flexibility of this hyperthermophile protein.

Distribution of Stability and Flexibility. Sac7d adopts a "chromo domain-like" fold (SCOP 54160), with an SH3 barrel capped by a C-terminal helix. The pattern of backbone mobility and stability observed in Sac7d is similar to that described for a number of mesophile SH3 proteins (*68*−*72*), except that the level of disorder observed in the connecting elements of Sac7d (two turns and a loop) is significantly less. This is due to the more compact structure of the thermophilic Sac7d, with the majority of the connecting elements being tight turns (Y8 to E11, and V26 to M29) and 3_{10} helices (D16 to K19, and E47 to D49). The largest loop in Sac7d contains only six residues (D35 to T40). Overall, the relaxation data indicate relatively minor deviations of the backbone order parameters from a mean of 0.80 ± 0.06 along the length of the protein up to E62. Such values are similar to those observed in the least flexible regions of similar-sized mesophile proteins (*44*, *68*−*70*, *73*, *74*). The relaxation data do not show any indication of unusual rigidity in this hyperthermophile protein. Similar results have been reported for rubredoxin (*63*).

The least stable and most mobile region of Sac7d on the nanosecond to picosecond time scale is the latter half of the C-terminal α-helix following E62. The helix was defined to the C-terminus in the NMR structure primarily because of hydrogen bonds indicated by the observation of NHs immediately after dissolving the protein in D_2O (*7*), although the exchange rates for these protons were relatively fast leading to small ΔG_{HX} values. Notably, the C-terminal helix was defined to R63 in the crystal structure of the Sac7d−DNA complex (*6*). Significant flexibility in the end of the C-terminal helix of the more thermostable Sso7d was also mentioned in a relaxation study of arginine side-chain motions of that protein (*75*), although no backbone mobility data were provided.

Hydrogen exchange and ^{15}N relaxation data show that the most stable and inflexible regions largely coincide. They include the first strand of the N-terminal β-ribbon, the 3_{10} helix preceding the β-sheet, the three strands of the sheet (with the center strand the most stable), and the initial half of the C-terminal helix which packs against the β-sheet. Most importantly, this region includes the DNA-binding site. One of the most interesting aspects of Sac7d−DNA binding is the intercalation of V26 and M29 side chains, which enforces a 66° kink in the DNA. The intercalating residues are positioned at the beginning and end of the type II tight turn (V26-G27-K28-M29) between the first and second strands of the stable β-sheet. The NHs of G27 and K28 are solvent-exposed and therefore cannot report on the stability of the turn. The NH of V26 is hydrogen-bonded to the carbonyl of M29, and the NH of M29 is hydrogen-bonded back to the CO of V26. Both of these show significantly slowed exchange rates relative to reference peptides with ΔG_{HX} of 2.4 and 3.4 kcal/mol, respectively. These are not as great as the free energies for the core and indicate that the turn is less stable. The generalized order parameters for the V26 and M29 NH vectors in the turn indicate that the position of the backbone in this important region is relatively inflexible on the nanosecond to picosecond time scale, although the errors in the relaxation data for G27 and K28 were significantly larger than the other NHs and were excluded from the analysis. The reason for this was not apparent but may indicate fluctuations in the structure of the turn. This is consistent with the small increase in imprecision in the NMR structure in this region (*7*), as well as the difference in the

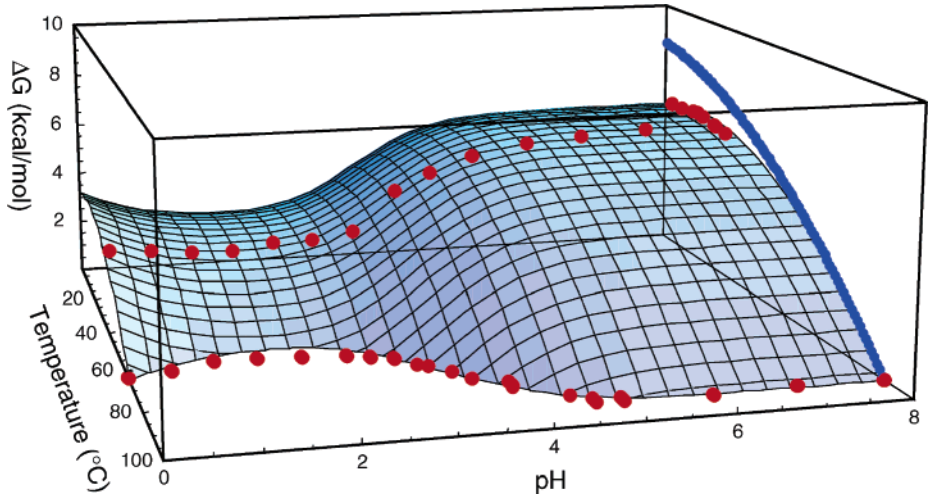

FIGURE 7: Amide hydrogen exchange free energies and T_m values for Sac7d overlayed onto the calculated free energy surface determined from global fitting of the linkage of folding on pH, temperature, and salt (*10*, *11*). Experimentally determined free energies of unfolding from hydrogen exchange data are shown with red circles on the surface and have been decreased by 1.0 kcal/mol to allow for the effect of D_2O. Experimental T_m values from DSC are shown with red circles at the intersection of the surface with the base plane. For comparison, the stability curve predicted using a ΔC_P of 500 from the Kirchhoff analysis of DSC data is shown with the bold blue curve.

position of the turn in the crystal structure of the protein−DNA complex compared to that in the NMR solution structure of the protein alone (i.e., there is a 2 Å shift of Cα of K28 in the DNA complex toward the center of the protein and away from the DNA). In summary, the NMR structure and dynamics data are consistent with the DNA-binding β-sheet being the most stable region of the structure, with the tight turn containing the intercalating residues being less stable, possibly allowing for adjustment of the intercalating residues in the DNA complex.

Two-State Unfolding versus Local Instabilities. The unfolding of Sac7d has been fit with a two-state (N ↔ U) thermodynamic model to define parameters for global unfolding of the protein (*10*). A two-state model for protein folding is consistent with local instabilities since the model assumes that only two states are significantly populated (*28*, *76*). Local instabilities are associated with small changes in enthalpy (and *m*-values), and therefore, the populations of the locally unfolded species are not expected to change significantly with temperature (or denaturant). This is reflected by the exchange data for I20 and A44 in Figure 2. At high temperature or denaturant where global unfolding becomes significant, the local transitions are less important and unfolding is dominated by global denaturation. At low temperature or concentrations of denaturant, the extrapolated ΔG_{HX} values for the most stable core NHs depend significantly on the perturbant and are believed to correspond to the free energy of global two-state unfolding.

Protein Stability. The ΔG_{HX} measurements for the core residues provide a measure of the unfolding free energy of Sac7d which is independent of that obtained by thermal unfolding (*10*, *11*) and chemical denaturation (*12*). The results are consistent with the global linkage analysis and confirm the validity of the linkage approach in describing the stability of Sac7d (*10*). Like many proteins, Sac7d folding is promoted by anion binding at low pH, and a detailed study of the stability of Sac7d as a function of salt and pH indicated that contributions from anion binding to thermodynamic measurements of stability were significant. This linkage is not included in a Kirchhoff analysis as often used to obtain the ΔC_p of unfolding from the dependence of ΔH on T_m (obtained by varying the pH below 5). Such an analysis indicated an anomalous ΔC_p of unfolding of 497 ± 20 (cal/deg)/mol (*12*). In contrast, a global fitting of the variation of DSC parameters and circular dichroism intensities as a function of temperature (0−100 °C), salt (0−0.3 M KCl), and pH (0−8) indicated that the ΔC_p of unfolding was 711 ± 19 (cal/deg)/mol (*10*, *11*). While these differences may appear small given the commonly accepted errors in ΔC_p (*19*), a 40% increase in ΔC_p leads to a significantly different protein stability curve and free energy surface (Figure 5). The temperature of maximal stability using a ΔC_p of 497 (cal/deg)/mol (and a T_m of 90.7 and ΔH of 58.5 kcal/mol from DSC) is predicted to occur at −9.4 °C with a $\Delta G°$ of 8.5 kcal/mol. The global analysis including linkage of chloride binding indicated a maximal stability at 17.4 °C with a $\Delta G°$ of 6.2 kcal/mol (*11*), which would correspond to 7.2 kcal/mol in HX due to D_2O stabilization. The free energy surface obtained from a global linkage analysis of Sac7d unfolding as a function of pH and temperature is shown in Figure 7. Overlayed on the surface are the temperature and pH dependence of ΔG_{HX} (red symbols on the surface) along with the pH dependence of the T_m (red symbols where the surface intersects the zero plane). The surface shows a "saddle" with a minimum near pH 2. This leads to not only an increase in T_m below pH 2 but also the increase in ΔG_{HX} at low pH. The maximum in the free energy surface as a function of temperature coincides with the maximum in ΔG_{HX}, and differs significantly from that predicted using the ΔC_P obtained from a conventional Kirchhoff analysis of DSC data (bold blue curve). The temperature and pH dependence of ΔG_{HX} are in excellent agreement with that obtained by the global linkage analysis and support a ΔC_p of unfolding of 711 ± 19 (cal/deg)/mol. The native state hydrogen exchange free energies independently demonstrate the validity of the global analysis of the linkage of anion and proton binding to folding.

Hyperthermophile Protein Stability Curves. One of the goals of obtaining rigorous measurements of thermophile protein stability is to define the structural parameters which

Table 2: Thermodynamic Parameters Characterizing the Reversible Unfolding of Selected Thermophile Proteins

protein	T_m (°C)	$\Delta H(T_m)$ (kcal/mol)	ΔC_P ((cal/deg)/mol)	ΔG_{max} (kcal/mol)	T_{max} (°C)	refs
Sac7d	90.1	58.5	711	7.2	17	*11*
RNase H	86	131	1800	12.7	20	*65*
Rubredoxin[a]	137	80	(500)	9.2	5	*64*
HpyA1[b]	110	172	2200	17.2	39	*62*
TmCsp	82	62.6	1100	4.8	29	*80*
TmCheY	101	94	1170	9.5	29	*56*
TmHU[c]	78	44	757	3.5	24	*58*
TmGDH	70	82.5	1400	6.7	16	*60*
$E2_{cd}$	73	216	3800	16.8	21	*81*

[a] The values for *Pyrococcus furiosus* rubredoxin are from recent NMR chemical exchange measurements using a protein with an amino terminal modification (A2K) that does not significantly alter the stability (*64*). These data indicated that the predicted T_m near 200 °C from earlier work (*82*) was probably incorrect due to the model peptide used for referencing the exchange of the cysteine NHs in the iron−sulfur center. The ΔC_P used here is an estimated value from ref *64*, since an experimental value has not been reported. [b] For the dimeric histone from *Pyrococcus*, the reference temperature is the $T°$, i.e., the T_m at 1 M protein. [c] The T_m and ΔG_{max} used for TmHU is that reported at 120 μM protein (*58*).

control the placement of the protein stability curve in these fascinating proteins (eq 4). As mentioned by a number of authors (*12*, *77*, *78*), enhanced protein stability can be obtained by (1) shifting the protein stability curve vertically with an increase in stability at all temperatures; (2) shifting the curve laterally to increase the temperature of maximal stability, T_{max}, without actually increasing the maximal stability of the protein; or (3) broadening the stability curve to increase the T_m. Thermodynamic studies of a large number (e.g., 42) of mesophile proteins indicated an average T_{max} of 12 °C (±19 °C) (*78*). The error in this number reflects to some extent the error in ΔC_P measurements. The stabilities of only a small number of hyperthermophile proteins have been characterized thermodynamically due to irreversible unfolding of most of the thermophile proteins studied to date. Thermodynamic parameters for a few well-characterized thermophile proteins which unfold reversibly are summarized in Table 2. The temperature of maximal stability, T_{max}, observed for Sac7d is 17 °C. This is identical (within 1 SD) to the average obtained for the thermophile proteins, viz., 22 (±10) °C. The average T_{max} observed for the thermophile proteins is not significantly different from that observed for mesophile proteins. The slightly higher average T_{max} observed by Rees and Robertson (*78*) results from the use of a smaller data set (and the inclusion of the hydrogen exchange data for rubredoxin which have been modified in recent work (*64*)). The data indicate that the forces available to enhance protein stability in hyperthermophiles do not permit a dramatic shifting of the temperature of maximal stability to higher temperature. This likely reflects the thermodynamics of the hydrophobic effect (*18*), although contributions from electrostatic interactions can perturb the position of T_{max} (*79*). While additional contributions to protein stability are important in stabilizing thermophile proteins, the major determinant of both mesophile and thermophile protein stability is expected to be the hydrophobic effect, and therefore, the maximum in the stability curves for both is expected to be near 20 °C.

REFERENCES

1. McAfee, J., Edmondson, S., Datta, P., Shriver, J., and Gupta, R. (1995) Gene cloning, sequencing, expression, and characterization of the Sac7 DNA-binding proteins from the extremely thermophilic archaeon *Sulfolobus acidocaldarius*, *Biochemistry 34*, 10063−10077.
2. McAfee, J. G., Edmondson, S., Zegar, I., and Shriver, J. W. (1996) Equilibrium DNA binding of Sac7d protein from the hyperthermophile *Sulfolobus acidocaldarius*: fluorescence and circular dichroism studies, *Biochemistry 35*, 4034−4045.
3. Edmondson, S. P., and Shriver, J. W. (2001) DNA binding proteins Sac7d and Sso7d from *Sulfolobus*, *Methods Enzymol. 334*, 129−145.
4. White, M. F., and Bell, S. D. (2002) Holding it together: chromatin in the archaea, *Trends Genet. 18*, 621−626.
5. Reeve, J. N. (2003) Archaeal chromatin and transcription, *Mol. Microbiol. 48*, 587−598.
6. Robinson, H., Gao, Y.-G., McCrary, B. S., Edmondson, S. P., Shriver, J. W. and Wang, A. H.-J. (1998) The hyperthermophile chromosomal protein Sac7d sharply kinks DNA, *Nature 392*, 202−205.
7. Edmondson, S. P., Qiu, L., and Shriver, J. W. (1995) Solution structure of the DNA-binding protein Sac7d from the hyperthermophile *Sulfolobus acidocaldarius*, *Biochemistry 34*, 13289−13304.
8. Shriver, J. W., Peters, W. B., Szary, N., Clark, A. T., and Edmondson, S. P. (2001) Calorimetric analyses of hyperthermophile proteins, *Methods Enzymol. 334*, 389−422.
9. Peters, W. B., Edmondson, S. P., and Shriver, J. W. (2004) Thermodynamics of DNA binding and distortion by the hyperthermophile chromatin protein Sac7d, *J. Mol. Biol. 343*, 339−360.
10. McCrary, B. S., Bedell, J., Edmondson, S. P., and Shriver, J. W. (1998) Linkage of protonation and anion binding to the folding of Sac7d, *J. Mol. Biol. 276*, 203−224.
11. Clark, A., McCrary, B. S., Edmondson, S., and Shriver, J. (2004) Thermodynamics of core hydrophobicity and packing in the hyperthermophile proteins Sac7d and Sso7d, *Biochemistry 43*, 2840−2853.
12. McCrary, B. S., Edmondson, S. P., and Shriver, J. W. (1996) Hyperthermophile protein folding thermodynamics: differential scanning calorimetry and chemical denaturation of Sac7d, *J. Mol. Biol. 264*, 784−805.
13. Tanford, C. (1970) Protein denaturation. Part C: theoretical models for the mechanism of denaturation, *Adv. Protein Chem. 24*, 1−95.
14. Pace, C. N. (1975) The stability of globular proteins, *CRC Crit. Rev. Biochem. 3*, 1−43.
15. Privalov, P. (1979) Stability of proteins. Small globular proteins, *Adv. Protein Chem. 33*, 167−241.
16. Becktel, W., and Schellman, J. (1987) Protein stability curves, *Biopolymers 26*, 1859−1877.
17. Sturtevant, J. (1987) Biochemical applications of differential scanning calorimetry, *Annu. Rev. Phys. Chem. 38*, 463−488.
18. Makhatadze, G., and Privalov, P. L. (1995) Energetics of protein structure, *Adv. Protein Chem. 47*, 308−425.
19. Robertson, A. D., and Murphy, K. P. (1997) Protein structure and the energetics of protein stability, *Chem. Rev. 97*, 1251−1267.
20. Lumry, R., Biltonen, R., and Brandts, J. (1966) Validity of the "two-state" hypothesis for conformational transitions of proteins, *Biopolymers 4*, 917−944.
21. Pace, C. N. (1986) Determination and analysis of urea and guanidine hydrochloride denaturation curves, *Methods Enzymol. 131*, 266−280.
22. Santoro, M., and Bolen, D. (1988) Unfolding free energy changes determined by the linear extrapolation method. 1. Unfolding of phenylmethanesulfonyl α-chymotrypsin using different denaturants, *Biochemistry 27*, 8063−8068.
23. Pace, C. N., Shirley, B., and Thomson, J. A. (1989) Measuring the conformational stability of a protein, in *Protein Structure: A Practical Approach* (Creighton, T. E., Ed.) pp 311−330, IRL Press, New York.
24. Freire, E. (1995) Thermal denaturation methods in the study of protein folding, *Methods Enzymol. 259*, 144−168.
25. Makhatadze, G. (1998) Measuring protein thermostability by differential scanning calorimetry, in *Current Protocols in Protein Science*, pp 7.9.1−7.9.14, John Wiley & Sons, New York.

26. Huyghues-Despointes, B. M., Scholtz, J. M., and Pace, C. N. (1999) Protein conformational stabilities can be determined from hydrogen exchange rates, *Nat. Struct. Biol. 6*, 910−912.
27. Straume, M., and Freire, E. (1992) Two-dimensional differential scanning calorimetry: simultaneous resolution of intrinsic protein structural energetics and ligand binding interactions by global linkage analysis, *Anal. Biochem. 203*, 259−268.
28. Bai, Y., Milne, J. S., Mayne, L., and Englander, S. W. (1994) Protein stability parameters measured by hydrogen exchange, *Proteins 20*, 4−14.
29. Englander, W., and Kallenbach, N. (1984) Hydrogen exchange and structural dynamics of proteins and nucleic acids, *Q. Rev. Biophys. 16*, 521−655.
30. Bai, Y., and Englander, S. W. (1996) Future directions in folding: the multi-state nature of protein structure, *Proteins 24*, 145−151.
31. Hilser, V. J., and Freire, E. (1996) Structure-based calculation of the equilibrium folding pathway of proteins. Correlation with hydrogen exchange protection factors, *J. Mol. Biol. 262*, 756−772.
32. Mayo, S., and Baldwin, R. L. (1993) Guanidinium chloride induction of partial unfolding in amide proton exchange in RNase A, *Science 262*, 873−876.
33. Chamberlain, A. K., Handel, T. M., and Marqusee, S. (1996) Detection of rare partially folded molecules in equilibrium with the native conformation of RNaseH, *Nat. Struct. Biol. 3*, 782−787.
34. Swint-Kruse, L., and Robertson, A. D. (1996) Temperature and pH dependence of hydrogen exchange and global stability for ovomucoid third domain, *Biochemistry 35*, 171−180.
35. Krishna, M. M., Hoang, L., Lin, Y., and Englander, S. W. (2004) Hydrogen exchange methods to study protein folding, *Methods 34*, 51−64.
36. Englander, S. W., Sosnick, T. R., Englander, J. J., and Mayne, L. (1996) Mechanisms and uses of hydrogen exchange, *Curr. Opin. Struct. Biol. 6*, 18−23.
37. Hvidt, A., and Nielsen, S. O. (1966) Hydrogen exchange in proteins, *Adv. Protein Chem. 21*, 287−386.
38. Roder, H., Wagner, G., and Wüthrich, K. (1985) Individual amide proton exchange rates in thermally unfolded basic pancreatic trypsin inhibitor, *Biochemistry 24*, 7407−7411.
39. Arrington, C. B., and Robertson, A. D. (2000) Kinetics and thermodynamics of conformational equilibria in native proteins by hydrogen exchange, *Methods Enzymol. 323*, 104−124.
40. Zhang, O., Kay, L. E., Olivier, J. P., and Forman-Kay, J. D. (1994) Backbone ^{1}H and ^{15}N resonance assignments of the N-terminal SH3 domain of drk in folded and unfolded states using enhanced-sensitivity pulsed field gradient NMR techniques, *J. Biomol. NMR 4*, 845−858.
41. Bedell, J. L., McCrary, B. S., Edmondson, S. P., and Shriver, J. W. (2000) The acid-induced folded state of Sac7d is the native state, *Protein Sci. 9*, 1878−1888.
42. Bai, Y., Milne, J. S., Mayne, L., and Englander, S. W. (1993) Primary structure effects on peptide group hydrogen exchange, *Proteins 17*, 75−86.
43. Bevington, P. R., and Robinson, D. K. (1992) *Data Reduction and Error Analysis for the Physical Sciences*, McGraw-Hill, New York.
44. Farrow, N. A., Muhandiram, R., Singer, A. U., Pascal, S. M., Kay, C. M., Gish, G., Shoelson, S. E., Pawson, T., Forman-Kay, J. D., and Kay, L. E. (1994) Backbone dynamics of a free and phosphopeptide-complexed Src homology 2 domain studied by ^{15}N NMR relaxation, *Biochemistry 33*, 5984−6003.
45. Korzhnev, D. M., Skrynnikov, N. R., Millet, O., Torchia, D. A., and Kay, L. E. (2002) An NMR experiment for the accurate measurement of heteronuclear spin-lock relaxation rates, *J. Am. Chem. Soc. 124*, 10743−10753.
46. Mandel, A. M., Akke, M., and Palmer, A. G., III (1995) Backbone dynamics of *Escherichia coli* ribonuclease HI: correlations with structure and function in an active enzyme, *J. Mol. Biol. 246*, 144−163.
47. Kay, L. E., Torchia, D. A., and Bax, A. (1989) Backbone dynamics of proteins as studied by ^{15}N inverse detected heteronuclear NMR spectroscopy: application to staphylococcal nuclease, *Biochemistry 28*, 8972−8979.
48. Tjandra, N., Feller, S., Pastor, R., and Bax, A. (1995) Rotational diffusion anisotropy of human ubiquitin from ^{15}N NMR relaxation, *J. Am. Chem. Soc. 117*, 12568−12566.
49. Schurr, J. M., Babcock, H. P., and Fujimoto, B. S. (1994) A test of the model-free formulas. Effects of anisotropic rotational diffusion and dimerization, *J. Magn. Reson., Ser. B 105*, 211−224.
50. Lipari, G., and Szabo, A. (1982) Model-free approach to the interpretation of nuclear magnetic resonance relaxation in macromolecules, *J. Am. Chem. Soc. 104*, 4546−4559.
51. Clore, G. M., Driscoll, P. C., Wingfield, P. T., and Gronenborn, A. M. (1990) Deviations from the simple two-parameter model-free approach to the interpretation of nitrogen-15 nuclear magnetic relaxation in proteins, *J. Am. Chem. Soc. 112*, 4989−4991.
52. Jaenicke, R., and Böhm, G. (1998) The stability of proteins in extreme environments, *Curr. Opin. Struct. Biol. 8*, 738−748.
53. Jaenicke, R. (2000) Do ultrastable proteins from hyperthermophiles have high or low conformational rigidity?, *Proc. Natl. Acad. Sci. U.S.A. 97*, 2962−2964.
54. Blake, P., Park, J., Bryant, F., Aono, A., and Magnuson, J. K. (1991) Determinants of protein hyperthermostability. 1. Purification, amino acid sequence, and secondary structure from NMR of the rubredoxin from the hyperthermophilic archaebacterium *Pyrococcus furiosus*, *Biochemistry 30*, 10885−10895.
55. Henning, M., Darimont, B., Sterner, R., Kirschner, K., and Jansonius, J. N. (1995) 2.0 Å structure of indole-3-glycerol phosphate synthase from the hyperthermophile *Sulfolobus solfataricus*: possible determinants of protein stability, *Structure 3*, 1295−1306.
56. Deutschman, W. A., and Dahlquist, F. W. (2001) Thermodynamic basis for the increased thermostability of CheY from the hyperthermophile *Thermotoga maritima*, *Biochemistry 40*, 13107−13113.
57. Dams, T., and Jaenicke, R. (1999) Stability and folding of dihydrofolate reductase from the hyperthermophilic bacterium *Thermotoga maritima*, *Biochemistry 38*, 9169−9178.
58. Ruiz-Sanz, J., Filimonov, V. V., Christodoulou, E., Vorgias, C. E., and Mateo, P. L. (2004) Thermodynamic analysis of the unfolding and stability of the dimeric DNA-binding protein HU from the hyperthermophilic eubacterium *Thermotoga maritima* and its E34D mutant, *Eur. J. Biochem. 271*, 1497−1507.
59. Lebbink, J. H., Consalvi, V., Chiaraluce, R., Berndt, K. D., and Ladenstein, R. (2002) Structural and thermodynamic studies on a salt-bridge triad in the NADP-binding domain of glutamate dehydrogenase from *Thermotoga maritima*: cooperativity and electrostatic contribution to stability, *Biochemistry 41*, 15524−15535.
60. Consalvi, V., Chiaraluce, R., Giangiacomo, L., Scandurra, R., Christova, P., Karshikoff, A., Knapp, S., and Ladenstein, R. (2000) Thermal unfolding and conformational stability of the recombinant domain II of glutamate dehydrogenase from the hyperthermophile *Thermotoga maritima*, *Protein Eng. 13*, 501−507.
61. Zaiss, K., and Jaenicke, R. (1999) Thermodynamic study of phosphoglycerate kinase from *Thermotoga maritima* and its isolated domains: reversible thermal unfolding monitored by differential scanning calorimetry and circular dichroism spectroscopy, *Biochemistry 38*, 4633−4639.
62. Li, W.-T., Grayling, R., Sandman, K., Edmondson, S., Shriver, J. W., and Reeve, J. N. (1998) Thermodynamic stability of archaeal histones, *Biochemistry 37*, 10563−10572.
63. Hernandez, G., Jenney, F. E., Jr., Adams, M. W., and LeMaster, D. M. (2000) Millisecond time scale conformational flexibility in a hyperthermophile protein at ambient temperature, *Proc. Natl. Acad. Sci. U.S.A. 97*, 3166−3170.
64. LeMaster, D. M., Tang, J., and Hernandez, G. (2004) Absence of kinetic thermal stabilization in a hyperthermophile rubredoxin indicated by 40 microsecond folding in the presence of irreversible denaturation, *Proteins 57*, 118−127.
65. Hollien, J., and Marqusee, S. (1999) A thermodynamic comparison of mesophilic and thermophilic ribonucleases H, *Biochemistry 38*, 3831−3836.
66. Hollien, J., and Marqusee, S. (1999) Structural distribution of stability in a thermophilic enzyme, *Proc. Natl. Acad. Sci. U.S.A. 96*, 13674−13678.
67. Butterwick, J. A., Patrick Loria, J., Astrof, N. S., Kroenke, C. D., Cole, R., Rance, M., and Palmer, A. G., III (2004) Multiple time scale backbone dynamics of homologous thermophilic and mesophilic ribonuclease HI enzymes, *J. Mol. Biol. 339*, 855−871.
68. Hansson, H., Mattsson, P. T., Allard, P., Haapaniemi, P., Vihinen, M., Smith, C. I., and Hard, T. (1998) Solution structure of the SH3 domain from Bruton's tyrosine kinase, *Biochemistry 37*, 2912−2924.

69. Ferreon, J. C., Volk, D. E., Luxon, B. A., Gorenstein, D. G., and Hilser, V. J. (2003) Solution structure, dynamics, and thermodynamics of the native state ensemble of the Sem-5 C-terminal SH3 domain, *Biochemistry 42*, 5582−5591.
70. Wang, C., Pawley, N. H., and Nicholson, L. K. (2001) The role of backbone motions in ligand binding to the c-Src SH3 domain, *J. Mol. Biol. 313*, 873−887.
71. Horita, D. A., Zhang, W., Smithgall, T. E., Gmeiner, W. H., and Byrd, R. A. (2000) Dynamics of the Hck-SH3 domain: comparison of experiment with multiple molecular dynamics simulations, *Protein Sci. 9*, 95−103.
72. Mittermaier, A., and Kay, L. E. (2004) The response of internal dynamics to hydrophobic core mutations in the SH3 domain from the Fyn tyrosine kinase, *Protein Sci. 13*, 1088−1099.
73. Schneider, D., Dellwo, M., and Wand, A. J. (1992) Fast internal main-chain dynamics of human ubiquitin, *Biochemistry 31*, 3645−3652.
74. Tillett, M. L., Blackledge, M. J., Derrick, J. P., Lian, L. Y., and Norwood, T. J. (2000) Overall rotational diffusion and internal mobility in domain II of protein G from *Streptococcus* determined from ^{15}N relaxation data, *Protein Sci. 9*, 1210−1216.
75. Berglund, H., Baumann, H., Knapp, S., Ladenstein, R., and Hard, T. (1995) Flexibility of an arginine side chain at a DNA−protein interface, *J. Am. Chem. Soc. 117*, 12883−12884.
76. Chu, R. A., Takei, J., Barchi, J. J., Jr., and Bai, Y. (1999) Relationship between the native-state hydrogen exchange and the folding pathways of barnase, *Biochemistry 38*, 14119−14124.
77. Nojima, H., Ikai, A., Oshima, T., and Noda, H. (1977) Reversible thermal unfolding of thermostable phosphoglycerate kinase. Thermostability associated with mean zero enthalpy change, *J. Mol. Biol. 116*, 429−442.
78. Rees, D. C., and Robertson, A. D. (2001) Some thermodynamic implications for the thermostability of proteins, *Protein Sci. 10*, 1187−1194.
79. Makhatadze, G. I., Loladze, V. V., Gribenko, A. V., and Lopez, M. M. (2004) Mechanism of thermostabilization in a designed cold shock protein with optimized surface electrostatic interactions, *J. Mol. Biol. 336*, 929−942.
80. Wassenberg, D., Welker, C., and Jaenicke, R. (1999) Thermodynamics of the unfolding of the cold-shock protein from *Thermotoga maritima*, *J. Mol. Biol. 289*, 187−193.
81. Beadle, B. M., Baase, W. A., Wilson, D. B., Gilkes, N. R., and Shoichet, B. K. (1999) Comparing the thermodynamic stabilities of a related thermophilic and mesophilic enzyme, *Biochemistry 38*, 2570−2576.
82. Hiller, R., Zhou, Z., Adams, M. W. W., and Englander, S. W. (1997) Stability and dynamics in a hyperthermophile protein with melting temperature close to 200 °C, *Proc. Natl. Acad. Sci. U.S.A. 94*, 11329−11332.

BI051167D